Available online at www.sciencedirect.com
SCIENCE DIRECT®
Earth and Planetary Science Letters 243 (2006) 463–475
EPSL
www.elsevier.com/locate/epsl

New Early to Middle Triassic U–Pb ages from South China: Calibration with ammonoid biochronozones and implications for the timing of the Triassic biotic recovery

Maria Ovtcharova [a], Hugo Bucher [b,*], Urs Schaltegger [a], Thomas Galfetti [b], Arnaud Brayard [b], Jean Guex [c]

[a] *Department of Mineralogy, University of Geneva, rue des Maraîchers 13, CH-1205 Geneva, Switzerland*
[b] *Institute and Museum of Paleontology, University of Zürich, Karl Schmid-Strasse 4, CH-8006 Zürich, Switzerland*
[c] *Institute of Geology, University of Lausanne, BFSH2, CH-1015 Lausanne, Switzerland*

Received 24 September 2005; received in revised form 11 January 2006; accepted 23 January 2006
Available online 3 March 2006
Editor: V. Courtillot

Abstract

New zircon U–Pb ages are proposed for late Early and Middle Triassic volcanic ash layers from the Luolou and Baifeng formations (northwestern Guangxi, South China). These ages are based on analyses of single, thermally annealed and chemically abraded zircons. Calibration with ammonoid ages indicate a 250.6±0.5 Ma age for the early Spathian *Tirolites*/*Columbites* beds, a 248.1±0.4 Ma age for the late Spathian *Neopopanoceras haugi* Zone, a 246.9±0.4 Ma age for the early middle Anisian *Acrochordiceras hyatti* Zone, and a 244.6±0.5 Ma age for the late middle Anisian *Balatonites shoshonensis* Zone. The new dates and previously published U–Pb ages indicate a duration of ca. 3 my for the Spathian, and minimal durations of 4.5±0.6 my for the Early Triassic and of 6.6+0.7/−0.9 my for the Anisian. The new Spathian dates are in a better agreement with a 252.6±0.2 Ma age than with a 251.4±0.3 Ma age for the Permian–Triassic boundary. These dates also highlight the extremely uneven duration of the four Early Triassic substages (Griesbachian, Dienerian, Smithian, and Spathian), of which the Spathian exceeds half of the duration of the entire Early Triassic. The simplistic assumption of equal duration of the four Early Triassic subdivisions is no longer tenable for the reconstruction of recovery patterns following the end Permian mass extinction.

Keywords: U–Pb ages; zircon; Early Triassic; ammonoids; biotic recovery

1. Introduction

Following the biggest mass extinction of the Phanerozoic, the Early Triassic biotic recovery is generally assumed to have had a longer duration than that of other major mass extinctions. Understanding the mode and tempo of the recovery requires calibration of high-resolution biochronozones based

* Corresponding author. Fax: +41 44 634 49 23.
E-mail addresses: maria.ovtcharova@terre.unige.ch (M. Ovtcharova), Hugo.FR.Bucher@pim.unizh.ch (H. Bucher), urs.schaltegger@terre.unige.ch (U. Schaltegger), jean.guex@unil.ch (J. Guex).

0012-821X/$ - see front matter © 2006 Elsevier B.V. All rights reserved.
doi:10.1016/j.epsl.2006.01.042

on the maximal association principle [1] with high-resolution radio-isotopic ages. Mass extinctions are usually followed by a survival phase and a recovery phase before ecosystems become fully re-organized, i.e. until diversity reaches a new equilibrium phase. For the Early Triassic, proposed estimates for the duration of the survival and recovery phases are so far not constrained by primary (i.e. non-interpolated) radio-isotopic ages (see compilation by [2]). Moreover, as indicated by the Early Triassic ammonoid recovery, the leading taxonomic group for correlation of Mesozoic marine rocks, the return to a new equilibrium phase was not a smooth, gradual process. The recovery underwent several fluctuations and was severely set back during end Smithian time [3]. Calibrating such diversity fluctuations by means of U–Pb ages is critical for a better understanding of the various abiotic and biotic factors that shaped the recovery, and for the improvement of the geological time scale, as well.

Based on the unrivaled North American ammonoid record, Tozer [4] and Silberling and Tozer [5] introduced four Early Triassic stages: Griesbachian, Dienerian, Smithian, and Spathian, in ascending order. In 1992, a decision of the Subcommission of Triassic Stratigraphy downgraded these four stages to substages to adopt the Russian two-stage subdivisions scheme, i.e. the Induan and Olenekian stages as originally defined by [6]. However, the global correlation of the boundary between these two stages still poses problems because these are defined within two different realms, the Induan within the Tethyan Realm, and the Olenekian within the Boreal Realm. The Induan stage correlates approximately with the Griesbachian and the Dienerian, whereas the Olenekian stage correlates approximately with the Smithian and the Spathian. Here, we deliberately use the scheme of Tozer which by far best reflects global ammonoid faunal changes during the Early Triassic. Whether Tozer's subdivisions should be ranked at the stage or substage level remains a minor, essentially formalistic point. Essential is the construction of a high resolution faunal succession permitting objective correlation of distant basins.

Only a few calibrations between isotopic and paleontological ages are available for the Early and Middle Triassic. U–Pb ages ranging from 253 [7] to ca. 251 Ma [8] have been proposed for the Permian–Triassic boundary. The U–Pb age for the Anisian–Ladinian boundary is of ca. 241 Ma [9,10]. Preliminary U–Pb ages of 247.8 Ma are available for the base of the early Anisian, and of 246.5 Ma for the early middle Anisian [11,12]. This leaves a 10 to 12 my interval for the Early Triassic (Griesbachian, Dienerian, Smithian, and Spathian) and the Anisian stage, whose respective boundaries are primarily defined by changes in ammonoid faunas. Due to the lack of absolute age constraints, extrapolation or interpolation of the respective durations of the Early Triassic stages or substages and of the Anisian are usually based on the flawed assumption of equal duration of zones or subzones (e.g., [13], p. 284). Recent simulations have demonstrated that this assumption is even more unrealistic for extinction and recovery phases [14], which stresses again the need for radio-isotopic age calibrations during such biological crises. With increasing knowledge of Early Triassic and Anisian ammonoid faunas, the number of zones reflecting newly documented faunas intercalated between those previously known is rapidly growing ([15] for the synthesis of the Anisian from North America; [16] and ongoing work by Bucher and Guex for the Spathian). Because the number of zones or subzones reflects the combined effects of the completeness of the record, of sampling efforts, as well as the variable evolutionary rates in time and space, it cannot be used to interpolate the duration of zones or stages comprised between two calibration points, regardless what the distance of these points in time may be. Here, we report on four new U–Pb ages calibrated with the ammonoid-rich series of the Early Triassic and Anisian marine record of northwestern Guangxi (Fig. 1A) and their correlation with the North American ammonoid biochronozones.

2. Geological setting and ammonoid age control

The investigated volcanic ash layers were sampled from the Luolou Formation of Early Triassic age and from the overlying Baifeng Formation of Anisian age [17]. These formations belong to the Nanpanjiang Basin (see [18] for a synthesis) of the South China Block, which occupied an equatorial position during Early and Middle Triassic times as indicated by paleomagnetic data [19]. At its type locality, and in the Jinya, Leye and Wangmo areas, the Luolou Formation is composed of mixed carbonate-siliciclastic, ammonoid- and conodont-rich rocks deposited in an outer platform setting. As evidenced by ammonoid age control, most of the vertical facies changes within the 70 to 100 m thick Luolou Fm. (Fig. 1B) are synchronous within a 100 km long, NW–SE oriented belt extending from Wangmo (southern Guizhou) to Leye and Fengshan (northwestern Guangxi, see Fig. 1A).

Two coarse-grained volcanic ash layers (CHIN-10 and CHIN-23, see Fig. 1B) consistently occur within the upper, carbonate unit of Spathian age of the Luolou Fm.

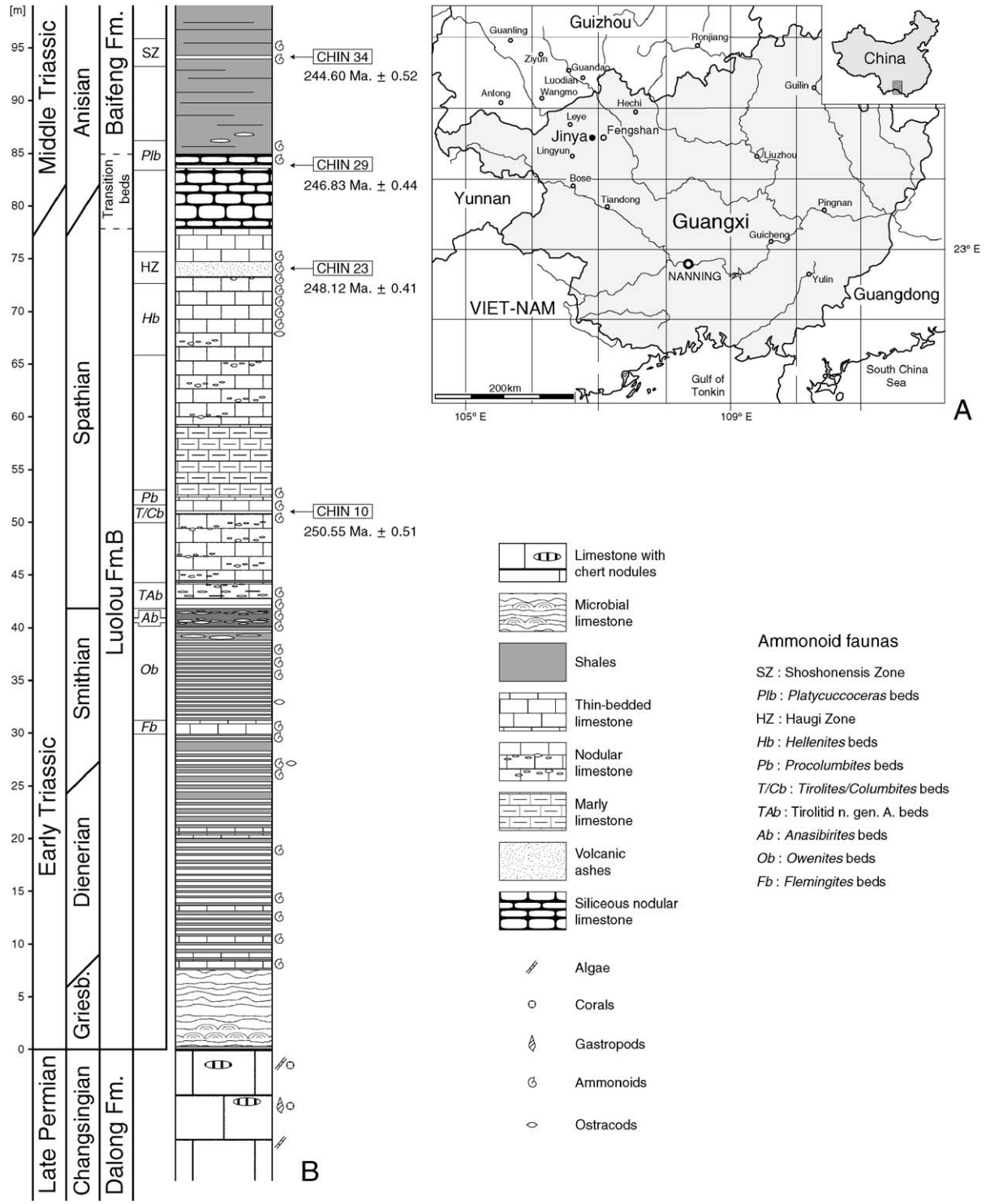

Fig. 1. (A) Location map of the various localities mentioned in the text. (B) Jinya section showing the stratigraphic position of the analyzed ash beds, and sample numbers with U–Pb ages obtained in this work. GPS coordinates of samples: CHIN-10 (N24°36′26.2″; E106°52′39.6″), CHIN-23 (N24°36′48.9″; E106°52′34.0″), CHIN-29 (N24°35′25.8″; E106°52′09.7″), CHIN-34 (N24°35′22.0″; E106°53′13.6″).

The lower, 15 to 25 cm thick ash layer (CHIN-10) shows a remarkable lateral continuity between the Jinya and Wangmo areas, over a distance of ~100 km. The upper, 60 to 260 cm thick ash layer (CHIN-23) can be traced laterally from Jinya to Leye (~60 km). The *Tirolites*/*Columbites* ammonoid assemblage associated with CHIN-10 indicates an early Spathian age (see Fig. 2). This fauna has a global, low-paleolatitudinal distribution. It is known from numerous Tethyan localities, as well as from the plate-bound Union Wash Formation (California) and the Thaynes Formation (Idaho). The low-paleolatitudinal *Neopopanoceras haugi* Zone fauna, associated with CHIN-23, is diagnostic of a late Spathian age (Fig. 2) and correlates with the high-paleolatitudinal *Keyserlingites subrobustus* Zone [20]. The *N. haugi* Zone is well documented in the Union Wash Formation (eastern California) and the Prida Formation (northwestern Nevada). It is here first reported from South China.

Transition from the Luolou Fm. to the overlying Baifeng Fm. is marked by a conspicuous, approximately 10 m thick unit composed of nodular siliceous limestones (i.e. "Transition beds" in Fig. 1B), which occurs in the Leye, Jinya, and Tiandong areas (see Fig. 1A), The "Transition beds" indicate a generalized drowning of the basin and contain abundant volcanic ash layers. Among these, a unique 25 cm thick, four-event ash layer (CHIN-29, see Fig. 1A) is intercalated within the uppermost part of the unit. It has been recognized in Jinya as well as in the vicinity of Tiandong, more than 200 km to the South. In the Jinya area, the poorly preserved, *Platycuccoceras*-dominated ammonoid assemblage (*Platycuccoceras* sp. indet., *Acrochordiceras* cf. *A. hyatti*, *Pseudodanubites* sp. indet.) associated with CHIN-29 indicates an early middle Anisian age (*A. hyatti* Zone, [21]).

The Baifeng Formation consists of a siliciclastic, thickening and coarsening upward turbiditic succession whose minimal thickness exceeds 1000 m. The predominantly shaly base of the formation contains rare, thin (mm to cm) medium-grained ash layers. One of these (CHIN-34, see Fig. 1B) is bracketed by layers containing a late middle Anisian ammonoid assemblage diagnostic of the low-paleolatitudinal *Balatonites shoshonensis* Zone [22]. So far, no clear high-paleolatitudinal correlative of this zone has been recognized [15].

The drastic change of the sedimentary regime between the Luolou and Baifeng formations suggests a concomitant modification in directions or rates of the convergence between the South and North China blocks [19]. It is worth noting that the higher abundance of volcanic ash layers observed in the "Transition beds" coincides with this profound change in the sedimentary regime. A reduced sedimentation rate within the "Transition beds" could also lead to this apparent concentration of volcanic ash layers.

3. Isotopic ages of the Early Triassic and the Anisian

The Permian–Triassic boundary was first radioisotopically dated by [23] at Meishan (stratotype of the Permian/Triassic boundary, South China) by SHRIMP ion microprobe techniques. Zircons from the so-called "boundary clay" (a 5 cm thick bentonite layer, bed 25 in [24] in Meishan yielded an age of 251.2±3.4 Ma. The same bentonite contains sanidine which has been dated by $^{40}Ar/^{39}Ar$ analysis to 249.9±0.2 Ma [25] (all further cited U–Pb and Ar–Ar ages do not include uncertainties on decay constants, tracer calibrations, natural standards and flux monitors). Subsequently, Bowring et al. [8] dated a succession of ash beds closely bracketing the Permian–Triassic boundary in three South Chinese sections (Meishan, Heshan, and Laibin) by multiple and single zircon grain U–Pb analyses. These authors placed the boundary at 251.4±0.3 Ma, excluding a concordant cluster consisting of 5 multi-grain analyses at an age of 252.7±0.4 Ma from their calculation (assuming inheritance of slightly older grains, perhaps incorporated during eruption). Mundil et al. [7] emphasized biases generated by the averaging effect resulting from multiple crystal analyses in [8] and proposed an age of 253 Ma for the boundary exclusively based on new and previous single grain analyses from the Meishan ash beds. Recently, Mundil et al. [26] proposed a revised age of 252.6±0.2 Ma for the Permian–Triassic boundary. Here, we emphasize the fact that for a comparison between ages derived from different isotopic systems, systematic errors have to be taken into a account. Recent studies [27,28] indicate that $^{40}Ar/^{39}Ar$ ages are generally younger (by ca. 1%) than U–Pb ages.

Only preliminary U–Pb ages exist for the early Anisian and the base of the middle Anisian [11,12]. However, an assessment of these data is impossible since details have not been published. Accordingly, these authors [11] emphasized that their dates "should not be cited as certain boundary ages". These two preliminary dates are from ash layers intercalated within slope series of Early and Middle Triassic age (Guandao sections in southern Guizhou) regarded as an equivalent of the Luolou Fm. by [11]. Paleontological age constraints are provided by conodonts (Orchard, in [11], Fig. 17). The older age of 247.8 Ma is associated

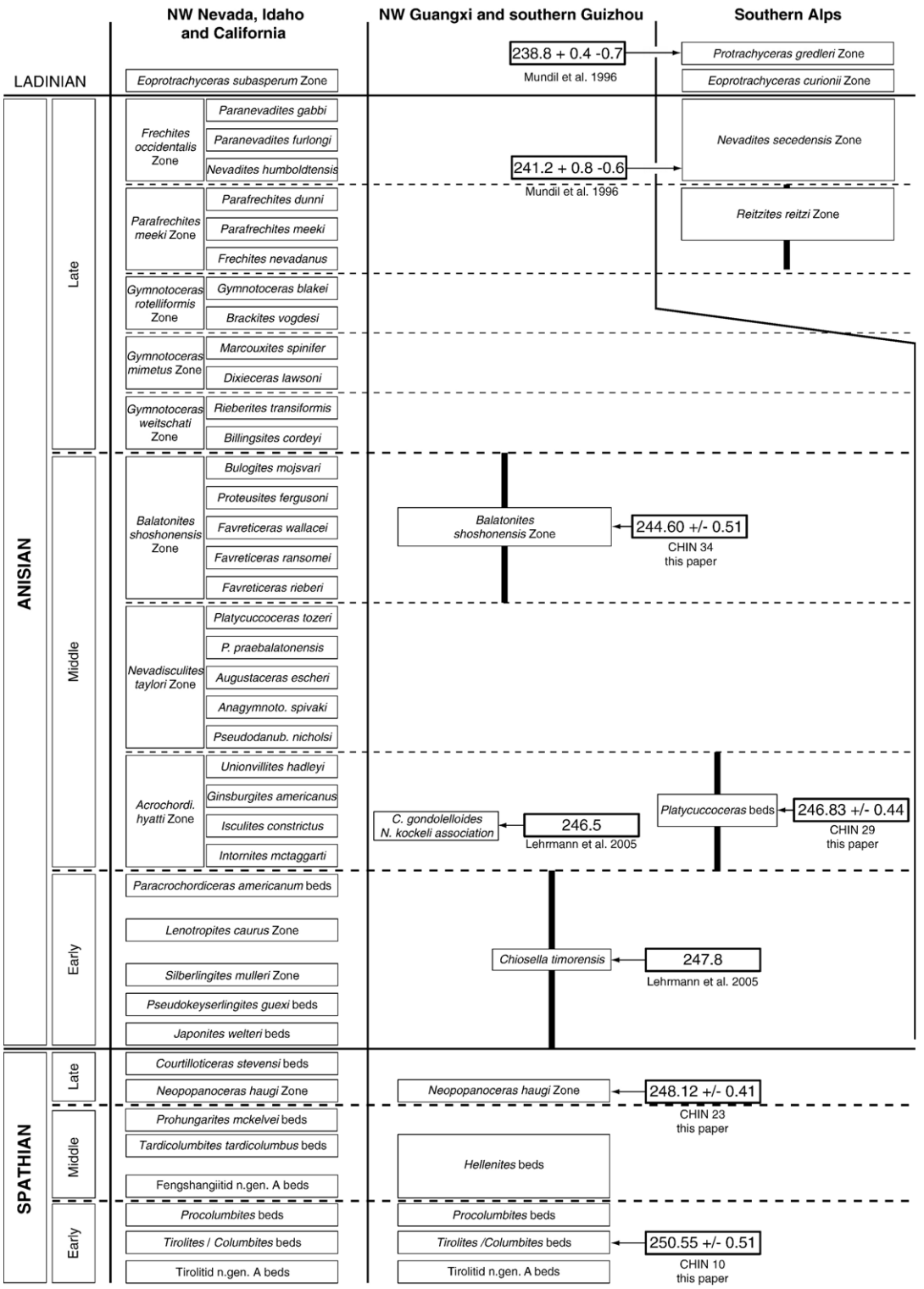

Fig. 2. Calibration of all new and published Early and Middle Triassic U–Pb ages from northwestern Guangxi, southern Guizhou, and the southern Alps with local ammonoid or conodont ages. Uncertainties in the biochronological correlations between the high-resolution North American ammonoid zonation and the Chinese and Alpine paleontological ages calibrated with U–Pb ages are indicated by the vertical black bars. See text for further explanation.

with *Chiosella timorensis*, whose range is restricted to the early Anisian in Nevada and elsewhere (Orchard, personal communication 2005). In the Guandao sequence, the two other associated conodonts, *Chiosella gondolelloides* and *Neogondolella regalis*, range higher into the early middle Anisian (Orchard, personal communication 2005) and are thus of less value in trying to narrow down the paleontological age. Hence, this first age falls within the early Anisian, but cannot be precisely tied to any of the refined ammonoid zones or beds as revised by Monnet and Bucher [15]. So far, this age is the only one that provides an upper limit for the Early–Middle Triassic boundary. The younger age of 246.5 Ma is associated with *C. gondolelloides*, *Nicoraella germanicus*, and *Nicoraella kockeli.* In the Nevadan ammonoid sequence, the overlap of *N. germanicus* with *N. kockeli* is only seen in the *Isculites constrictus* Subzone of the *A. hyatti* Zone (Orchard, personal communication 2005), which is early middle Anisian in age.

The next younger available radio-isotopic ages in the Triassic time scale are around the Anisian–Ladinian boundary in the Southern Alps, where tuff layers are bracketed by ammonoid faunas [9,29]. Based on U–Pb analyses of single zircon crystals, Mundil et al. [30] and Brack et al. [31] dated the base of the *Nevadites secedensis* Zone (late Anisian) to 241.2±0.8 Ma and the *Protrachyceras gredleri* Zone (Ladinian) to 238.8+0.5/−0.2 Ma. By interpolation, they proposed an age of 240.7 Ma for the base of the *Eoprotrachyceras curionii* Zone, which is the oldest Ladinian Zone [29]. Palfy et al. [10] used the U–Pb method on multiple zircon grain fractions to date tuff layers intercalated with faunas they considered to be near the Anisian–Ladinian boundary in the Balaton Highlands (Hungary). As a result, they proposed an age of 240.5±0.5 Ma for the base of *Reitzites reitzi* Zone in Hungary. However, as shown by [7], multigrain analyses are prone to yield inaccurate, generally younger ages, as a result of unrecognized Pb loss. Based on the above results, Ogg ([13], Fig. 17.1) extrapolated an age of 237±2 Ma for the Anisian–Ladinian boundary, which conflicts with the 238.8+0.5/−0.2 Ma age obtained for the Ladinian *P. gredleri* Zone.

4. U–Pb geochronological method and results

The most accurate available isotopic system for dating ash layers is the decay of ^{238}U and ^{235}U to radiogenic lead isotopes ^{206}Pb and ^{207}Pb in zircon. In undamaged zircon, the diffusion coefficients for Pb and U are negligible [32]. The analytical techniques of low-blank isotope-dilution thermal ionization mass spectrometry (ID-TIMS) applied to a number of single crystals from a zircon population of the same sample offer the possibility to date the crystallization of this population with permil uncertainty. Precise and accurate zircon ages can mainly be biased by three effects: (1) post-crystallization lead loss resulting from open system behaviour of crystal domains, which then yield apparently younger age; (2) incorporation of old cores acting as nuclei during crystallization,–or more generally–of foreign lead with a radiogenic composition indicative for a pre-ash depositional age, leading to too old apparent ages; (3) incorporation of xenocrysts (or "antecrysts") from a previous magmatic cycle, often slightly older than the original magmatic population and particularly common during multiple volcanic events.

Our U–Pb data indicate that the tuffs contain entirely magmatic grains yielding concordant results, as well as zircons with an important inherited component of Late Proterozoic age. The cathodoluminescence (CL) imaging revealed that there are grains with undisturbed oscillatory zoning patterns (OZPs), which are considered to be representative of magmatic growth (Fig. 3a). Some grains from the same sample, however, display a conspicuous discordant core, which may account for the presence of older inherited lead components (Fig. 3b). CL images may also show a distinct fainting of the OZP, indicating a replacement of the magmatic zoning by structureless high-luminescent zones (Fig. 3c). These processes are well-known to cause U–Pb interelement fractionation and lead loss (see, e.g., [33,34]).

4.1. Analytical technique

Zircons were prepared by standard mineral separation and purification methods (crushing and milling, concentration via Wilfley Table or hand washing, magnetic separation, and heavy liquids). For each sample, least-magnetic zircon crystals were selected and mounted in epoxy resin and imaged by cathodoluminescence to assess whether the population contains inherited cores.

In order to minimize the effects of secondary lead loss two techniques were employed: (1) conventional air-abrasion [35] and (2) "CA (chemical abrasion)-TIMS" technique involving high-temperature annealing followed by a HF leaching step [36]. The latter has been shown to be more effective in removing strongly radiation damaged zircon domains, which underwent lead-loss during post crystallization fluid processes [26,36]. Air-abraded zircons were washed first in diluted HNO_3, followed by distilled water and acetone in an ultrasonic bath prior to weighing. For the zircons

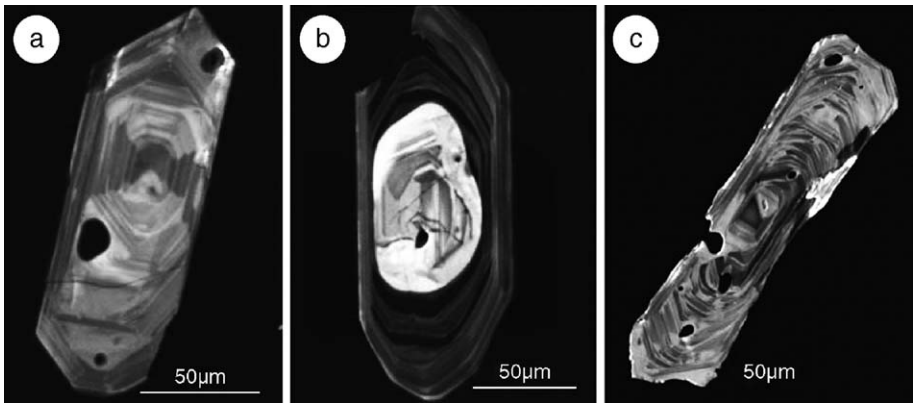

Fig. 3. Representative cathodoluminescence (CL) pictures of zircon: (a) undisturbed oscillatory zoning pattern (sample CHIN-29); (b) crystal with a core indicating the presence of an inherited lead component (sample CHIN-23); (c) oscillatory zoning with diffuse zone boundaries, indicating a disturbed lattice and therefore possible lead loss (sample CHIN-23).

subjected to chemical abrasion techniques, annealing was performed by loading 20–40 zircon grains of each sample in quartz crucibles and placing them into a furnace at 900 °C for approximately 60 h. Subsequently, for the leaching (chemical abrasion) step, zircons from each sample were transferred in 3 ml screw-top Savillex vials with ca. 120 μl concentrated HF. Loosely capped Savillex vials were arranged into a Teflon Parr™ vessel with 1 ml concentrated HF, and placed in an oven at 180 °C for 12–15 h. After the partial dissolution step, the leachate was completely pipetted out and the remaining zircons were fluxed for several hours in 6 N HCl (on a hotplate at a temperature of ca. 80 °C), rinsed in ultrapure H_2O and then placed back on the hot plate for an additional 30 min in 4 N HNO_3 for a "clean-up" step. The acid solution was removed and the fractions were again rinsed several times in ultra-pure water and acetone in an ultrasonic bath. Single zircons were selected, weighed and loaded for dissolution into pre-cleaned miniaturized Teflon vessels. After adding a mixed ^{205}Pb–^{235}U spike zircons were dissolved in 63 μl concentrated HF with a trace of 7 N HNO_3 at 180 °C for 5 days, evaporated and re-dissolved overnight in 36 μl 3 N HCl at 180 °C. Pb and U were separated by anion exchange chromatography in 40 μl micro-columns, using minimal amounts of ultra-pure HCl, and finally dried down with 3 μl 0.2 N or 0.06 N H_3PO_4.

Isotopic analysis was performed in ETH-Zurich on a MAT262 mass spectrometer equipped with an ETP electron multiplier backed by a digital ion counting system. The latter was calibrated by repeated analyses of the NBS 982 standard using the $^{208}Pb/^{206}Pb$ ratio of 1.00016 for mass bias correction [37] and the U500 standard, in order to correct for the 0.3% multiplier-inherent logarithmic rate effect [38]. Mass fractionation effects were corrected for 0.09±0.05 per a.m.u. Both lead and uranium were loaded with 1 μl of silica gel-phosphoric acid mixture [39] on outgassed single Re-filaments, and Pb as well as U (as UO_2) isotopes were measured sequentially on the electron multiplier. Total procedural common Pb concentrations were measured at values between 0.4 and 3.5 pg and were attributed solely to laboratory contamination. They were corrected with the following isotopic composition: $^{206}Pb/^{204}Pb$: 18.5 ±0.6% (1σ), $^{207}Pb/^{204}Pb$: 15.5±0.5% (1σ), $^{208}Pb/^{204}Pb$: 37.9±0.5% (1σ), representing the average values for 13 blank determinations in the Geneva laboratory 2004–2005. The uncertainties of the spike and blank lead isotopic composition, mass fractionation correction, and tracer calibration were taken into account and propagated to the final uncertainties of isotopic ratios and ages. The ROMAGE program was used for age calculation and error propagation (Davis, unpublished). The international R33 standard zircon [40] has been dated at an age of 420.7±0.7 Ma during the same analytical period (n=6). Calculation of concordant ages and averages was done with the Isoplot/Ex v.3 program of Ludwig [41]. Ellipses of concordia diagrams represent 2 sigma uncertainties.

4.2. Results

4.2.1. Sample CHIN-10

Zircons from sample CHIN-10 are short to long prismatic (up to 150 μm in their longest dimensions), often cracked, rich in apatite and fluid inclusions. CL zircon imaging revealed that there are grains with undisturbed oscillatory zoning, predominantly long

Table 1
U–Pb isotopic data of analyzed zircons

Sample no.	Weight (mg)	Concentration			Th/U[a]	Atomic ratios							Correlation coefficient	Ages		
		U (ppm)	Pb (ppm)	Pb com. (pg)		$^{206}Pb/^{204}Pb$[b]	$^{207}Pb/^{206}Pb$[c,d]	Error 2σ (%)	$^{207}Pb/^{235}U$[c]	Error 2σ (%)	$^{206}Pb/^{238}U$[c,d]	Error 2σ (%)		$^{206}Pb/^{238}U$	$^{207}Pb/^{235}U$	$^{207}Pb/^{206}Pb$
Chin-10																
1[e]	0.0024	378	16.28	2.62	0.45	888	0.051460	0.74	0.2812	0.94	0.03962	0.64	0.62	250.50	251.59	261.68
2[e]	0.0024	244	10.74	2.97	0.37	513	0.051330	0.78	0.2808	0.90	0.03968	0.44	0.50	250.83	251.29	255.58
3	0.0032	348	14.77	3.31	0.49	1027	0.051210	0.68	0.2791	1.34	0.03953	0.78	0.73	249.94	249.97	250.29
4	0.0010	194	10.22	2.45	0.56	226	0.053080	1.80	0.3030	2.06	0.04141	0.72	0.51	261.54	268.74	332.01
5	0.0032	345	14.83	0.60	0.63	4612	0.051320	0.24	0.2810	0.46	0.03971	0.36	0.86	251.03	251.43	255.15
6	0.0028	258	9.61	0.95	0.49	1712	0.051140	0.38	0.2481	0.52	0.03518	0.38	0.68	222.89	224.99	247.98
7	0.0031	78	3.33	0.49	0.61	1250	0.051210	0.62	0.2789	0.88	0.03950	0.58	0.71	249.74	249.78	250.17
8	0.0020	225	9.00	0.98	0.34	1159	0.051310	0.66	0.2799	0.86	0.03956	0.52	0.64	250.10	250.55	254.81
Chin-23																
9[e]	0.0039	438	17.73	0.88	0.46	4818	0.051190	0.46	0.2757	0.59	0.03907	0.44	0.64	247.05	247.26	249.25
10[e]	0.0045	241	9.89	1.94	0.43	1404	0.050950	0.48	0.2746	0.62	0.03910	0.46	0.64	247.22	246.40	238.53
11	0.0030	377	15.79	0.69	0.32	4335	0.051330	0.44	0.2960	0.94	0.04183	0.94	0.85	264.14	263.27	255.53
12	0.1010	260	10.02	2.04	0.24	3219	0.051120	0.22	0.2767	0.42	0.03925	0.38	0.85	248.20	248.00	246.15
13	0.0095	272	10.87	1.13	0.38	5707	0.051220	0.20	0.2771	0.40	0.03923	0.36	0.87	248.08	248.34	250.78
14	0.0055	410	16.48	1.51	0.40	3733	0.051200	0.22	0.2771	0.42	0.03925	0.36	0.85	248.18	248.32	249.73
15	0.0075	347	13.48	2.08	0.27	3132	0.051080	0.20	0.2761	0.62	0.03919	0.58	0.95	247.88	247.55	244.37
16	0.0051	188	7.36	0.98	0.31	2432	0.051160	0.48	0.2764	0.56	0.03918	0.48	0.58	247.78	247.79	247.91
17	0.0108	240	9.17	0.99	0.24	6545	0.051200	0.16	0.2772	0.42	0.03927	0.36	0.93	248.29	248.43	249.74
18	0.0180	95	21.49	0.68	0.13	34422	0.149840	0.10	4.4198	0.38	0.21393	0.33	0.97	1249.70	1716.00	2344.10
Chin-29																
19[e]	0.0013	172	24.67	1.48	0.63	957	0.069730	1.72	1.2208	1.86	0.12697	0.64	0.38	770.55	810.14	920.53
20[e]	0.0010	338	15.88	3.03	0.48	293	0.051320	1.56	0.2757	1.68	0.03896	0.54	0.38	246.36	247.21	255.25
21	0.0012	857	36.54	0.73	0.66	3484	0.051300	0.42	0.2758	0.50	0.03900	0.52	0.66	246.61	247.34	254.23
22	0.0033	264	10.85	0.88	0.52	2466	0.051190	0.34	0.2757	0.54	0.03906	0.44	0.78	246.99	247.22	249.41
23	0.0090	149	6.41	3.29	0.54	1023	0.051420	0.42	0.2766	0.60	0.03902	0.36	0.73	246.74	247.96	259.54
24	0.0010	279	11.67	0.62	0.58	1136	0.051130	0.68	0.2756	0.82	0.03907	0.42	0.56	247.19	247.15	246.78
25	0.0058	33	1.37	0.69	0.56	692	0.051170	0.98	0.2754	1.18	0.03904	0.48	0.58	246.88	247.03	248.46
Chin-34																
26[e]	0.0100	268	11.07	0.83	0.50	1044	0.051070	1.66	0.2707	1.78	0.03845	0.66	0.36	243.21	243.29	244.02
27[e]	0.0017	282	11.40	0.63	0.46	1441	0.051160	1.20	0.2719	1.39	0.03854	0.92	0.52	243.79	244.18	247.92
28	0.0020	338	13.81	1.81	0.51	1121	0.051100	0.70	0.2728	1.12	0.03872	0.60	0.84	244.87	244.91	245.39
29	0.0010	236	10.47	1.62	0.55	375	0.051050	1.26	0.2722	1.40	0.03867	0.44	0.46	244.58	244.42	242.88
30	0.0026	285	12.12	2.10	0.55	882	0.051110	0.50	0.2724	0.64	0.03865	0.34	0.63	244.45	244.57	245.73
31	0.0007	581	25.05	1.67	0.51	617	0.051030	0.68	0.2723	0.80	0.03870	0.46	0.53	244.75	244.51	242.16
32	0.0004	1114	59.83	3.57	0.66	168	0.051870	2.20	0.2700	2.38	0.03775	0.68	0.40	238.88	242.70	279.76

[a] Calculated on the basis of radiogenic $^{208}Pb/^{206}Pb$ ratios, assuming concordancy.

[b] Corrected for fractionation and spike.

[c] Corrected for fractionation, spike and blank.

[d] Corrected for initial Th disequilibrium, using an estimated Th/U ratio of 4 for the melt.

[e] Air-abraded zircons.

prismatic, needle-like crystals. Some short prismatic and sub-equant zircons contain inherited cores. Eight single long prismatic crystals (assuming undisturbed oscillatory zoning) were analyzed from this sample following the laboratory procedure outlined above (analytical data are given in Table 1). There is no difference in age obtained by zircons pre-treated by air-abrasion or chemical-abrasion. Two of the chemically abraded zircons yielded variably discordant dates—one is significantly older (analysis 4) and thus indicates the presence of inherited component; and the one (analysis 6) shows lead loss (Fig. 4a). The remaining data are concordant within analytical error and define a weighted mean $^{206}Pb/^{238}Pb$ age of 250.55±0.51 Ma (MSWD=0.7; Fig. 4a), which we consider to be the best estimate for the age of this ash bed associated with the *Tirolites*/*Columbites* beds (early Spathian).

4.2.2. Sample CHIN-23

Zircons from this sample are similar in size and morphology to those described above. The CL zircon images display a clear oscillatory zoning pattern which often shows diffuse contacts between neighboring zones ("fainting"), grading into a replacement of the magmatic zoning by structureless high-luminescent zones. The CL images also revealed the presence of a core and an oscillatory rim in some of the short prismatic crystals. Therefore, only single long-prismatic, to acicular crystals were selected for analysis. Nevertheless, two of the chemically abraded zircons (analyses 11 and 18) are older in age and assumed to represent xenocrysts or contain inherited components. Two air-abraded zircons (analyses 9 and 10) are slightly younger than the chemically abraded zircons (Fig. 4b). This is interpreted as a result of the more efficient chemical abrasion technique which allows complete removal of more internal zones that underwent diffusive lead loss. The remaining six chemically abraded zircons are perfectly concordant and define a weighted mean $^{206}Pb/^{238}Pb$ age of 248.12±0.41 Ma (MSWD=0.13; Fig. 4b). We consider this to be the best estimate for the age of these zircons and hence, of the ash bed intercalated within the *N. haugi* Zone (late Spathian).

4.2.3. Sample CHIN-29

Zircons from this sample vary from short to long prismatic (up to 150 μm in their longest dimensions).

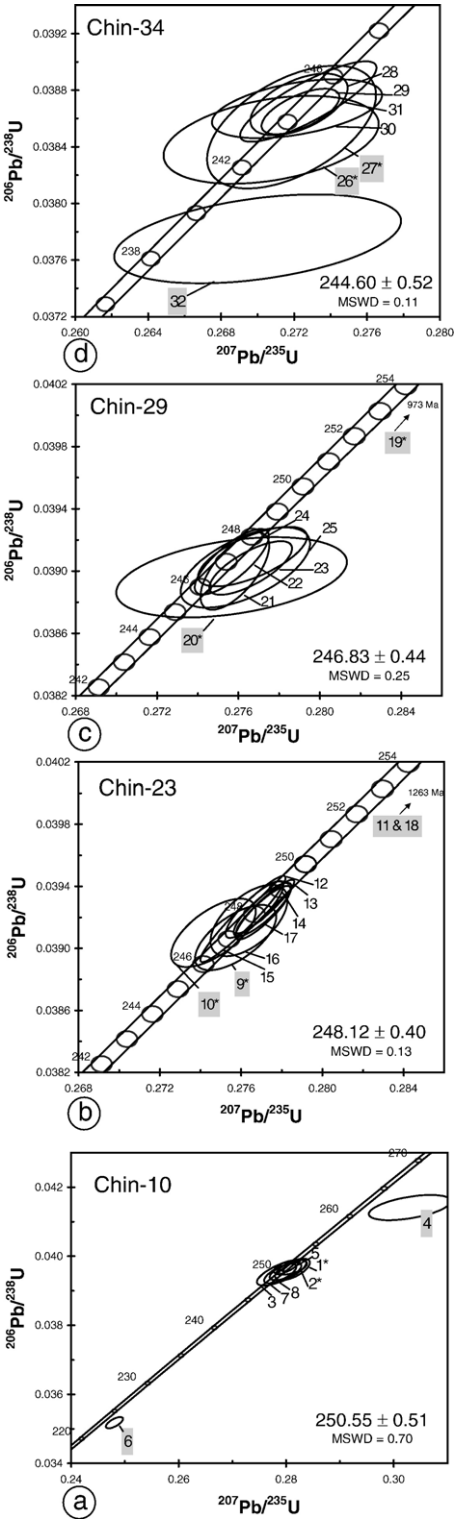

Fig. 4. Concordia plots showing the results of single-zircon analyses from volcanic ash bed samples, from the Jinya section (see Fig. 1B); (a) CHIN-10; (b) CHIN-23; (c) CHIN-29; (d) CHIN-34. Individual analyses are shown as 2σ error ellipses (grey numbers—analyses not included in weighted mean calculation; *—air-abraded zircons; the numbers correspond to the zircon numbers in Table 1). Given ages are weighted mean $^{206}Pb/^{238}U$ ages at 95% confidence level.

The CL imaging revealed that the large long prismatic or equant grains usually contain cores, whereas the needle-like crystals have usually magmatic oscillatory zoning. Air-abrasion of the latter is more difficult because they used to crack and disintegrate. Seven single long prismatic crystals (which would assumingly show undisturbed oscillatory zoning) were analyzed. There is no difference in age obtained by zircons pre-treated by air-abrasion or chemical-abrasion (Fig. 4c), except one of the air-abraded zircons (analysis 19), which is significantly older and thus indicates the presence of inherited component. The remaining data are concordant within analytical error and define a weighted mean $^{206}Pb/^{238}Pb$ age of 246.83±0.44 Ma (MSWD=0.25; Fig. 4c), which is interpreted to be the best estimate for the age of these zircons and inferentially the age of this ash bed associated with the *A. hyatti* Zone (early middle Anisian).

4.2.4. Sample CHIN-34

Zircons from this sample are larger than those in the previously described samples and range in size from 200×30 μm to short prismatic and rarely equant 50×50 μm grains. CL zircon imaging displays a clear oscillatory zoning pattern, which is often fainted, indicating some replacement or recrystallization process in the magmatic zones. CL also revealed the presence of cores and oscillatory rims in some of the short prismatic crystals, thus only single long prismatic, "needle-like" crystals were selected for analysis. Seven single grains were analyzed, all of which define a linear array on a concordia diagram and are anchored by four concordant analyses of chemically abraded zircons (Fig. 4d). Two air-abraded grains (analyses 26 and 27) are concordant within analytical error but slightly younger in age than the chemically abraded zircons and thus excluded from the calculation of the weighted mean $^{206}Pb/^{238}Pb$ age. Another of the chemically abraded zircons is also excluded from the mean, because it clearly shows effects of Pb loss (analysis 32). If only the most concordant four analyses are considered (analyses 28–31) a weighted mean $^{206}Pb/^{238}Pb$ age of 244.60±0.52 Ma (MSWD=0.11; Fig. 4d) is obtained. We consider this to be the age of the zircons and inferentially the age of the ash layer intercalated within the *B. shoshonensis* Zone (late middle Anisian).

5. Calibration of U–Pb ages and ammonoid zones

All new and previous dates are summarized in Fig. 2. All available U–Pb ages show a remarkable coherence, including the preliminary ages of [11]. The low-paleolatitudinal North American record provides the most comprehensive ammonoid succession for the Spathian and the Anisian, against which calibrated ages from South China and from the Southern Alps are correlated. The Anisian part of the North American zonation is derived from the recent synthesis of [15]. The Spathian part of the zonation is still in a preliminary stage ([16] and ongoing work by Bucher and Guex), but it correlates well with the faunal succession from the Luolou Fm. The poorer Anisian ammonoid record from the Baifeng Fm. can also be correlated, although with the obvious uncertainties as indicated by the black vertical bars (see Fig. 2).

The Early/Middle Triassic boundary is here now bracketed between 248.1±0.4 Ma and 247.8 Ma. With a *N. secedensis* Zone age of 241.2+0.8/−0.6 Ma [9], a minimal duration of 6.6+0.7/−0.9 my can be inferred for the Anisian. Considering a 252.6±0.2 Ma age for Permian/Triassic boundary [26] and a *N. haugi* Zone age of 248.1±0.4 Ma, the minimal duration of the Early Triassic amounts to 4.5±0.6 my. Alternatively, a Permian/Triassic boundary age of 251.4±0.3 Ma [8] would reduce the duration of the Early Triassic to 3.3 ±0.7 my. In this study, a minimum duration of 2.4 ±0.9 my is established for the Spathian. However, because the lowermost and uppermost Spathian ammonoid zones are not comprised within the interval bounded by our two U–Pb ages (see Fig. 2), a duration of ca. 3 my appears as a more realistic estimate. Regardless what the cumulative error on the Spathian duration may be, our results clearly highlight that the four Early Triassic substages are of extremely uneven duration. Consequently, the respective durations of the Induan and Olenekian stages are even more disparate. When taking all uncertainties of available U–Pb ages into account, a Permian–Triassic boundary of 251.4 ±0.3 Ma [8] implies that the minimal duration of the Spathian would represent 52% to unrealistic values in excess of 100% (!) of the entire Early Triassic. More realistically, a Permian–Triassic boundary of 252.6±0.2 Ma [26] implies that the minimal duration of the Spathian represents 41% to 95% of the entire Early Triassic.

6. Implications for the Early Triassic biotic recovery

Our calibration of new U–Pb ages with ammonoid zones implies that the use of stages or substages of supposedly equal duration irremediably leads to an exaggerated delayed recovery during the Early Triassic. The obvious consequence of the new calibrations is that

the survival and recovery phases of well-documented clades such as ammonoids [3], conodonts [42,43], or even brachiopods [44] must be significantly shorter than previous estimates.

As far as ammonoids are concerned [3], they return to a full diversity equilibrium in the Spathian, i.e. 1 to 3 my after the Permian–Triassic boundary, depending on which of the two available ages is considered for the latter. This equilibrium phase is characterized by a very steep, bimodal latitudinal gradient of taxonomic richness. Numerical simulations strongly support the fundamental causal link between the latitudinal gradient of sea-surface temperatures (SST) and the shape of the latitudinal gradient of taxonomic richness for marine organisms having at least one planktonic or pseudoplanktonic stage in their life-cycles [45]. Simply stated, a flat SST latitudinal gradient generates a low global diversity and a flat latitudinal diversity gradient, whereas a steep SST gradient generates a high global diversity and a steep, bimodal diversity gradient, similar to that of the Spathian ammonoids and to that of the present-day, Atlantic planktonic foraminifera used to calibrate the model in the simulations [45].

The transition leading from the Griesbachian low global diversity and flat latitudinal diversity gradient to the Spathian high global diversity and steep, bimodal diversity gradient was not a single, smooth and gradual rebound for the ammonoids [3]. It was interrupted during the end Smithian (the *Anasibirites pluriformis* Zone and its high paleolatitude correlative, the *Wasatchites tardus* Zone) by a sudden diversity collapse coupled with a drastic increase of cosmopolitan distributions, thus suggesting the resurgence of a flat SST gradient. The end Smithian ammonoid extinction also correlates with a global perturbation of the carbon cycle ([46,47]). It also coincides with the ultimate peak of anoxia in several Tethyan outer platforms ([46]). A warm and equal climate triggered by high concentrations of greenhouse gases appears as a likely explanation for such a flat SST gradient. Depending on the two alternative ages available for the Permian–Triassic boundary, the global end Smithian diversity drop of ammonoids can be inferred to have occurred no later than 0.5 my to 2.5 my after the beginning of the Triassic. However, a 0.5 my duration is evidently too short to accommodate all the ammonoid zones included into the Griesbachian, Dienerian, and Smithian substages.

More speculatively, it is tempting to relate these end Smithian events to a late volcanic pulse which would have occurred after the main eruption of the Siberian traps. $^{40}Ar/^{39}Ar$ ages of the huge basaltic flows from the Siberian Craton, the West Siberian Basin, Taimyr, and even possibly Kazakstan indicate that the main eruptive phase lasted no longer than 1 or 2 my [48–51]. Yet, genetically related, less intensive igneous activity at the southern fringe of the Siberian Craton apparently continued at least some 6 my after the main volcanic pulse [52]. A late eruptive activity in the Western Siberian Basin was also suggested by magnetostratigraphic constraints [53]. We also note that relevant information on the age of the youngest volcanic flows is extremely sparse, mainly because the upper boundary of the traps is either erosional and/or capped by terrestrial, poorly dated Triassic sediments. An upper age limit for the cessation of the main flood-volcanic event is nevertheless provided by a U–Pb baddeleyite age of 250.2±0.3 Ma from a carbonatite intruding the Guli volcanic-intrusive complex in the Maymecha-Kotuy area [54]. In the eastern Taimyr Peninsula (Chernokhrebetnaya River), Sobolev (personal communication 2005) documented that the oldest Early Triassic ammonoids within the Vostochnyi-Taymir Formation are of early Smithian age and occur 120 m above the uppermost basaltic flows of the Tsvekovomys Formation. This ammonoid age constraint apparently supports a short duration (1 to 2 my) for the main eruptive phase and the hypothesis that the end Smithian events must have been triggered by a distinct, later episode.

7. Conclusions

Our new Early Triassic dates indicate that the duration of the Spathian (ca. 3 my) amounts to at least half of the duration of the Early Triassic. The four Early Triassic substages are therefore of extremely uneven duration, not to mention the case of the Induan and the Olenekian stages. A minimal duration of $6.6+0.7/-0.9$ my is also proposed for the Anisian stage.

Our results confirm that U–Pb ages obtained from thermally annealed/chemically abraded zircons show improved concordancy, thus corroborating the results of [26,36]. This indicates that the chemical abrasion technique is obviously more efficient in removing Pb loss zones than air abrasion. This is more important in zircon populations consisting of acicular and skeletal grains, which are not well suited for thorough air-abrasion. However, zircon grains with undisturbed oscillatory zoning pattern represent a stable crystalline state and yielded comparable age results for both preparation techniques.

Our new U–Pb ages provide reliable tie points for the timing of the Triassic recovery. However, additional calibration points are needed for the Griesbachian,

Dienerian and Smithian substages. The new Spathian U–Pb ages also narrow the time interval between the end Smithian global diversity drop of ammonoids and the coeval carbon cycle perturbation on one hand, and the end of the main eruptive phase of the Siberian traps on the other. However, the timing of the ammonoid recovery and the age constraint from eastern Taimyr suggest that the end Smithian events were triggered by a later–yet unknown–volcanic pulse distinct from the main eruptive phase.

Acknowledgements

P. Brack, P.A. Hochuli and N. Goudemand are thanked for their thorough comments on an earlier version of the manuscript. Constructive reviews by the three EPSL referees R. Mundil, S. Kamo and N. Silberling were deeply appreciated. Kuang Guodun provided invaluable assistance in the field. M. Orchard shared useful information on the calibration between Anisian conodonts and ammonoids. E. Sobolev and V. Pavlov helped with the Russian literature on the Siberian traps. E. Sobolev also shared information on the Triassic stratigraphy of eastern Taimyr. A. von Quadt and M.-O. Diserens are thanked for helping with mass spectrometry and electron microscopy. U–Pb analyses were supported by the Swiss NSF project 200021-103335 (to U.S.). Fieldwork and paleontological work was supported by the Swiss NSF project 200020-105090/1 (to H.B) and a Rhône-Alpes-Eurodoc grant (to A.B). The Association Franco-chinoise pour la Recherche Scientifique et Technique (PRA T99-01) supported an initial field survey in Guangxi.

References

[1] J. Guex, Biochronologic Correlations, Springer-Verlag, 1991, p. 252.
[2] D.H. Erwin, S.A. Bowring, Y. Yin, End-Permian mass extinctions: a review, Spec. Pap.-Geol. Soc. Am. 356 (2002) 363–383.
[3] A. Brayard, H. Bucher, G. Escarguel, Diversity gradients of Early Triassic ammonoids and their paleoclimatic significance, Sixth International Symposium Cephalopods—Present and Past, Fayetteville, Arkansas, 2004.
[4] E.T. Tozer, A standard for Triassic Time, Bull.-Geol. Surv. Can. 156 (1967) 1–103.
[5] N.J. Silberling, E.T. Tozer, Biostratigraphic classification of the marine Triassic in North America, Spec. Pap.-Geol. Soc. Am. 110 (1968) 1–63.
[6] L.D. Kiparisova, Y.D. Popov, Subdivision of the lower series of the Triassic System into stages, Trans. Acad. Sci. USSR, Nauka 109 (1956) 842–845.
[7] R. Mundil, I. Metcalfe, K.R. Ludwig, P.R. Renne, F. Oberli, R. S. Nicoll, Timing of the Permian–Triassic biotic crisis: implications from new zircon U/Pb age data (and their limitations), Earth Planet. Sci. Lett. 187 (2001) 131–145.
[8] S.A. Bowring, D.H. Erwin, Y.G. Jin, M.W. Martin, K. Davidek, W. Wang, U/Pb zircon geochronology and tempo of the End-Permian mass extinction, Science 280 (1998) 1039–1045.
[9] P. Brack, H. Rieber, A. Nicora, The Global Boundary Stratotype Section and Point (GSSP) for the base of the Ladinian Stage (Middle Triassic). A proposal for the GSSP at the base of the Curionii Zone in the Bagolino section (Southern Alps, Northern Italy), Albertiana 28 (2003) 13–25.
[10] J. Palfy, R.R. Parrish, K. David, A. Vöros, Mid-Triassic integrated U–Pb geochronology and ammonoid biochronology from the Balaton Highland (Hungary), J. Geol. Soc. 160 (2003) 271–284.
[11] D.J. Lehrmann, J.L. Payne, P. Enos, P. Montgomery, J. Wei, Y. Yu, J. Xiao, M.J. Orchard, Field excursion 2: Permian–Triassic boundary and a Lower–Middle Triassic boundary sequence on the Great Bank of Guizhou, Nanpanjiang basin, southern Guizhou Province, Albertiana 33 (2005) 169–186.
[12] M.V. Martin, D.J. Lehrmann, S.A. Bowring, P. Enos, J. Ramenazi, J. Wei, J. Zhang, Anonymous, Timing of Lower Triassic carbonate bank buildup and biotic recovery following the end-Permian extinction across the Nanpanjiang Basin, South China, Abstr. Programs-Geol. Soc. Am. 33 (2001) 201.
[13] J.G. Ogg, The Triassic period, in: F.M. Gradstein, J.G. Ogg, A.G. Smith (Eds.), A Geological Time Scale, Cambridge Univ. Press, 2004, pp. 271–306.
[14] G. Escarguel, H. Bucher, Counting taxonomic richness from discrete biochronozones of unknown duration: a simulation, Palaeogeogr. Palaeoclimatol. Palaeoecol. 202 (2004) 181–208.
[15] C. Monnet, H. Bucher, Anisian (Middle Triassic) ammonoids from North America: quantitative biochronology and biodiversity, Stratigraphy 2 (2005) 281–296.
[16] J. Guex, A. Hungerbühler, J. Jenks, D. Taylor, H. Bucher, Dix-huit nouveaux genres d'ammonites du Spathien (Trias inférieur) de l'Ouest américan (Idaho, Nevada, Californie), Note préliminaire, Bull. Géol. Lausanne 362 (2005) 1–31.
[17] GXBGMR, (Guangxi, Bureau of Geology and Mineral Resources), Regional Geology of Guangxi Zhuang Autonomous Region, Geol. Mem. ser. 1 n. 3, Geol. Publ. House, Beijing, 1985, p. 853.
[18] D.J. Lehrmann, P. Enos, J.L. Payne, P. Montgomery, J. Wei, Y. Yu, J. Xiao, M.J. Orchard, Permian and Triassic depositional history of the Yangtze platform and Great Bank of Guizhou in the Nanpanjiang basin of Guizhou and Guangxi, south China, Albertiana 33 (2005) 149–168.
[19] S.A. Gilder, R.S. Coe, H.R. Wu, G.D. Kunag, X.X. Zhao, Q. Wu, Triassic paleomagnetic data from South China and their bearing on the tectonic evolution of the western Circum-Pacific Region, Earth Planet. Sci. Lett. 131 (1995) 269–287.
[20] H. Bucher, Lower Anisian ammonoids from the Northern Humboldt Range (Northwestern Nevada, USA) and their bearing upon the Lower–Middle Triassic boundary, Eclogae Geol. Helv. 82 (1989) 945–1002.
[21] H. Bucher, Ammonoids of the Hyatti Zone and the Anisian transgression in the Triassic Star Peak Group, Northwestern Nevada, USA, Palaeontogr. Abt. A 223 (1992) 137–166.
[22] H. Bucher, Ammonoids of the Shoshonensis Zone (Middle Anisian, Middle Triassic) from northwestern Nevada (USA), Jahrb. Geol. Bundesanst., Wien 135 (1992) 425–465.

[23] J.C. Claoué-Long, Z. Zhang, M. Guogan, D. Shaohua, The age of the Permian–Triassic boundary, Earth Planet. Sci. Lett. 105 (1991) 182–190.
[24] H.F. Yin, K.X. Zhang, J.N. Tong, Z.Y. Yang, S.B. Wu, The Global Stratotype Section and Point (GSSP) of the Permian–Triassic Boundary, Episodes 24 (2001) 102–114.
[25] P.R. Renne, Z.C. Zhang, M.A. Richards, M.T. Black, A.R. Basu, Synchrony and causal relations between Permian–Triassic Boundary crises and Siberian flood volcanism, Science 269 (1995) 1413–1416.
[26] R. Mundil, K.R. Ludwig, I. Metcalfe, P.R. Renne, Age and timing of the Permian mass extinctions: U/Pb dating of closed-system zircons, Science 305 (2004) 1760–1763.
[27] K. Min, R. Mundil, P.R. Renne, K.R. Ludwig, A test for systematic errors in 40Ar/39Ar geochronology through comparison with U/Pb analysis of a 1.1-Ga rhyolite, Geochim. Cosmochim. Acta 64 (2000) 73–98.
[28] P.R. Renne, R. Mundil, K. Min, K.R. Ludwig, Intercalibration of the U–Pb and Ar-40/Ar-39 geochronometers: status, prognosis, and proscription, Geochim. Cosmochim. Acta 69 (2005) A321.
[29] P. Brack, H. Rieber, R. Mundil, A. Nicora, The Global Boundary Stratotype Section and Point (GSSP) of the Ladinian Stage (Middle Triassic) at Bagolino (Southern Alps, Northern Italy) and its implications for the Triassic time scale, Episodes 28 (2005) 233–244.
[30] R. Mundil, P. Brack, M. Meier, H. Rieber, F. Oberli, High resolution U–Pb dating of Middle Triassic volcaniclastics: time-scale calibration and verification of tuning parameters for carbonate sedimentation, Earth Planet. Sci. Lett. 141 (1996) 137–151.
[31] P. Brack, R. Mundil, F. Oberli, M. Meier, H. Rieber, Biostratigraphic and radiometric age data question the Milankovitch characteristics of the Latemar cycles (southern Alps, Italy), Geology 24 (1996) 371–375.
[32] D.J. Cherniak, E.B. Watson, Pb diffusion in zircon, Chem. Geol. 172 (2001) 5–24.
[33] U. Schaltegger, C.M. Fanning, D. Gunther, J.C. Maurin, K. Schulmann, D. Gebauer, Growth, annealing and recrystallization of zircon and preservation of monazite in high-grade metamorphism: conventional and in-situ U–Pb isotope, cathodoluminescence and microchemical evidence, Contrib. Mineral. Petrol. 134 (1999) 186–201.
[34] P.W.O. Hoskin, U. Schaltegger, The composition of zircon and igneous and metamorphic petrogenesis, Zircon, Rev. Mineral. Geochem., Min. Soc. Am. 53 (2003) 27–62.
[35] T.E. Krogh, Improved accuracy of U–Pb zircon dating by selection of more concordant fractions using a high-gradient magnetic separation technique, Geochim. Cosmochim. Acta 46 (1982) 631–635.
[36] J.M. Mattinson, Zircon U–Pb chemical abrasion ("CA-TIMS") method: combined annealing and multi-step partial dissolution analysis for improved precision and accuracy of zircon ages, Chem. Geol. 220 (2005) 47–66.
[37] W. Todt, R.A. Cliff, A. Hanser, A.W. Hofmann, Evaluation of a 202Pb–205Pb double spike for high-precision lead isotope analysis, in: A. Basu, S. Hart (Eds.), Earth Processes: Reading the Isotopic Code, Am. Geophys. Union Monograph, vol. 95, 1996, pp. 429–437.
[38] S. Richter, S.A. Goldberg, P.B. Mason, A.J. Traina, J.B. Schwieters, Linearity tests for secondary electron multipliers used in isotope ratio mass spectrometry, Int. J. Mass Spectrom. 206 (2001) 105–127.
[39] H. Gerstenberger, G. Haase, A highly effective emitter substance for mass spectrometric Pb isotope ratio determinations, Chem. Geol. 136 (1997) 309–312.
[40] L.P. Black, S.L. Kamo, C.M. Allen, D.W. Davis, J.N. Aleinikoff, J.W. Valley, R. Mundil, I.H. Campbell, R.J. Korsch, I.S. Williams, C. Foudoulis, Improved Pb-206/U-238 microprobe geochronology by the monitoring of a trace-element-related matrix effect; SHRIMP, ID-TIMS, ELA-ICP-MS and oxygen isotope documentation for a series of zircon standards, Chem. Geol. 205 (2004) 115–140.
[41] K. Ludwig, Isoplot/Ex. V. 3., USGS Open-File Rep (2005).
[42] M.J. Orchard, Multielement conodont apparatuses of Triassic Gondolelloidea, Spec. Pap. Palaeontol. 73 (2005) 1–29.
[43] M.J. Orchard, On the explosive ratiation of Lower Triassic conodonts: a new multielement perspective, Albertiana 33 (2005) 65.
[44] Z.Q. Chen, K. Kaiho, A.D. George, Early Triassic recovery of the brachiopod faunas from the end-Permian mass extinction: a global review, Palaeogeogr. Palaeoclimatol. Palaeoecol. 224 (2005) 270–290.
[45] A. Brayard, G. Escarguel, H. Bucher, Latitudinal gradient of taxonomic richness: combined outcome of temperature and geographic mid-domains effects? J. Zoolog. Syst. Evol. Res. 43 (2005) 178–188.
[46] T. Galfetti, H. Bucher, A. Brayard, K. Guodun, V. Atudorei, P.A. Hochuli, H. Weissert, J. Guex, Biotic recovery and paleoclimate in Early Triassic times as reflected in carbonate carbon isotopes, sedimentary evolution and ammonoid fauna: records from South China and North India, in: F. Buzek, M. Novák (Eds.), 6th Int. Symp. Appl. Isotope. Geochem. Czech Geol. Surv., Prague, 2005, p. 268.
[47] J.L. Payne, D.J. Lehrmann, J.Y. Wei, M.J. Orchard, D.P. Schrag, A.H. Knoll, Large perturbations of the carbon cycle during recovery from the end-Permian extinction, Science 305 (2004) 506–509.
[48] V.E. Courtillot, P.R. Renne, On the ages of flood basalt events, C. R. Géosci. 335 (2003) 113–140.
[49] A.D. Saunders, R.W. England, M.K. Relchow, R.V. White, A mantle plume origin for the Siberian traps: uplift and extension in the West Siberian Basin, Russia, Lithos 79 (2005) 407–424.
[50] M.K. Reichow, A.D. Saunders, R.V. White, M.S. Pringle, A.I. Al'Mukhamedov, A.I. Medvedev, N.P. Kirda, Ar-40/Ar-39 dates from the West Siberian Basin: Siberian flood basalt province doubled, Science 296 (2002) 1846–1849.
[51] J.J. Lyons, R.S. Coe, X.X. Zhao, P.R. Renne, A.Y. Kazansky, A. E. Izokh, L.V. Kungurtsev, D.V. Mitrokhin, Paleomagnetism of the early Triassic Semeitau igneous series, eastern Kazakstan, J. Geophys. Res., [Solid Earth] 107 (B7) (2002) 1–15.
[52] A.V. Ivanov, S.V. Rasskazov, G.D. Feoktistov, H.Y. He, A. Boven, Ar-40/Ar-39 dating of Usol'skii sill in the south-eastern Siberian Traps Large Igneous Province: evidence for long-lived magmatism, Terra Nova 17 (2005) 203–208.
[53] M. Westphal, E.L. Gurevitch, B.V. Samsonov, H. Feinberg, J.P. Pozzi, Magnetostratigraphy of the lower Triassic volcanics from deep drill SG6 in western Siberia: evidence for long-lasting Permo-Triassic volcanic activity, Geophys. J. Int. 134 (1998) 254–266.
[54] S.L. Kamo, G.K. Czamanske, Y. Amelin, V.A. Fedorenko, D.W. Davis, V.R. Trofimov, Rapid eruption of Siberian flood-volcanic rocks and evidence for coincidence with the Permian–Triassic boundary and mass extinction at 251 Ma, Earth Planet. Sci. Lett. 214 (2003) 75–91.